

## INVESTIGATION OF MATERIAL PROPERTIES BY MEANS OF MAGNETIC METHODS

J. R a s e k, Z. S t o k ł o s a

**Institute of Material Science  
University of Silesia**

Bankowa 12, 40-007 Katowice, Poland

In the present paper, magnetic method of determination of ferrite content in austenite steels, based on saturation polarisation and magnetic polarisation of ferrite near the remanence point, have been presented for Fe-Cr-Ni-type alloys. Magnetic phase analysis, taking into account the distribution of total magnetic losses on eddy current losses, relaxation losses and hysteresis losses, have been discussed for low-carbon and low-alloy steels. The formulas on tangent angle of eddy current, hysteresis and relaxation (additional) losses have been presented. General formulas for magnetic permeability and coercive force have also been presented in terms of internal magnetic and material parameters. These parameters allowed to analyse the structural changes in magnetic materials. Examples of the influence of chemical composition, structural defects and thermal annealing on the changes of saturation polarisation, magnetic permeability, coercive force, magnetic hysteresis and relaxation losses have been discussed for low-carbon steels and amorphous alloys.

### 1. INTRODUCTION

Iron alloys, due to their universality and good mechanical properties, are fundamental constructional materials in engineering and water, motor, railway transport and in the power industry. On the other hand, iron alloys are mostly ferromagnetic. Therefore to the diagnose the machinery made from these alloys, magnetic methods, beside other methods, can be used. For that purpose magnetic physical properties, sensitive to the real structure of materials, are used. Magnetic properties sensitive to structure are, among other things, initial and maximum magnetic permeability, coercive force, magnetisation, magnetic hysteresis losses, eddy current losses, relaxation losses. Magnetic methods can be used to determine the contents of phases in the alloys based on iron and to analyse the changes of the real structure. The systems based on measuring of the magnetic permeability, saturation magnetic polarisation, leakage magnetic field and magnetic losses analysis are used. The calculation methods of leakage magnetic field, based on the numerical solution of the Poisson equations of magnetic vector potential are developed [1, 2].

A few examples of application of magnetic methods have been presented and the changes of selected magnetic quantities under the influence of chemical composition, the real structure and heat treatment, have been presented in the present paper.

## 2. DETERMINATION OF THE FERRITE CONTENT IN AUSTENITE ALLOYS

Figure 1 presents the phase diagram of Fe-Cr-Ni alloys according to their chemical composition. The chromium equivalent  $Cr_E$  depends on the content of ferrite-forming elements according to the equation:

$$(2.1) \quad Cr_E = 1 \times \%Cr + 1 \times \%Mo + 1.5 \times \%Si + 0.5 \times \%Nb.$$

The nickel equivalent  $Ni_E$  depends on the content of austenite-forming elements according to the equation:

$$(2.2) \quad Ni_E = 1 \times \%Ni + 30 \times \%C + 30 \times \%N + 0.5 \times \%Mn.$$

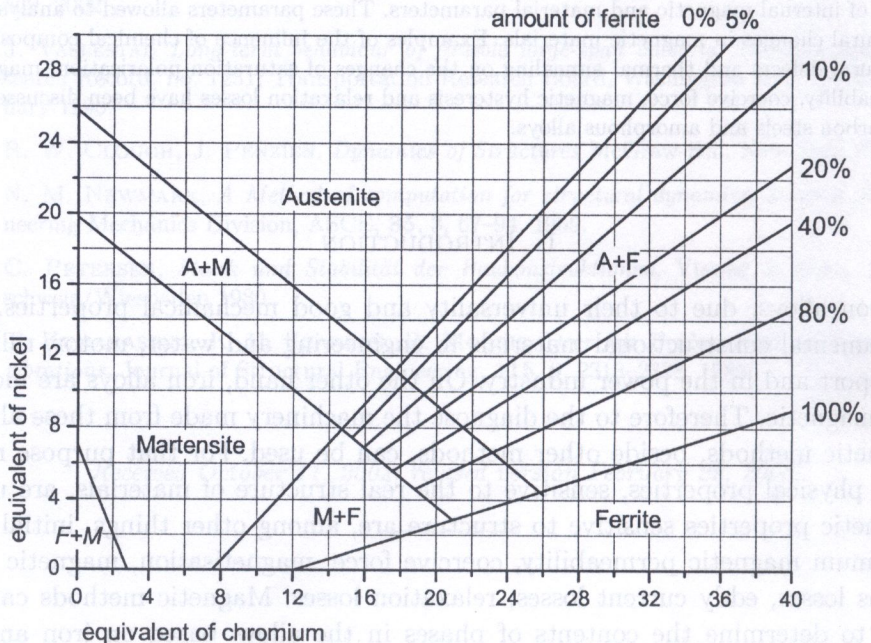


FIG. 1. Phase composition of Fe-Cr-Ni alloys [3].

The presence of ferrite phase (2–8%) is required in elements working at elevated temperatures in welded joints in the power industry, and to get suitable plasticity

in water transport. The percentage content of ferrite in the austenite alloys can be obtained by formula:

$$(2.3) \quad \% \text{ of ferrite} = \frac{j_w}{J_{sf} - J_a} \cdot 100 \%,$$

where  $J_{sf}$  is the saturation magnetic polarisation of the ferrite,  $J_a$  is the magnetic polarisation of the austenite phase in magnetic field  $\mu_0 H = 2.31 \cdot 10^{-4}$  T,  $V_p$  is the volume of material, and  $j_w$  is the dipole magnetic moment.

The saturation magnetic polarisation of the ferrite depends on chemical composition. Usually, in the first approximation, the linear dependence of particular elements is:

$$(2.4) \quad J_{sf} = 2.16 - 0.32\%C - 0.41\%N - 0.077\%Si - 0.03\%Mo - 0.02\%Mn - 0.04\%Cr - 0.034\%Ni - 0.18\%W - 0.16\%Ti \quad (\text{in teslas}).$$

The resultant magnetic dipole moment  $j_w$  can be determined by magnetometer method or by applying the magnetic balance. In the second case we can use the dependence:

$$(2.5) \quad F = j_w \frac{\partial H}{\partial z},$$

where  $F$  is the force acting on the sample in magnetic field with the gradient  $\partial H/\partial z$ , which can be determined by applying pure nickel or iron. Figure 2 presents the dipole magnetic moment on volume unit as a function of ferrite concentration obtained by applying magnetic balance. This dependence is linear in the range of up to about 11% of ferrite. Concentration of ferrite can also be obtained from the leakage magnetic field near the remanence point according to the formula:

$$(2.6) \quad \% \text{ of ferrite} = \frac{j_r}{V_p \cdot J_{rf}} \cdot 100\%,$$

where  $j_r$  is the resultant magnetic dipole moment near the remanence point,  $J_{rf}$  is the magnetic polarisation of ferrite near the remanence point, and  $V_p$  is the volume of the sample.

Magnetic polarisation  $J_{rf}$  is connected with the saturation magnetic polarisation of ferrite by means of the formula:

$$(2.7) \quad J_{rf} = C \cdot J_{sf}.$$

Hence, concentration of ferrite:

$$(2.8) \quad \% \text{ of ferrite} = \frac{j_r}{V_p \cdot C \cdot J_{sf}} \cdot 100\%,$$

where  $C$  is the factor dependent on geometry of the sample.

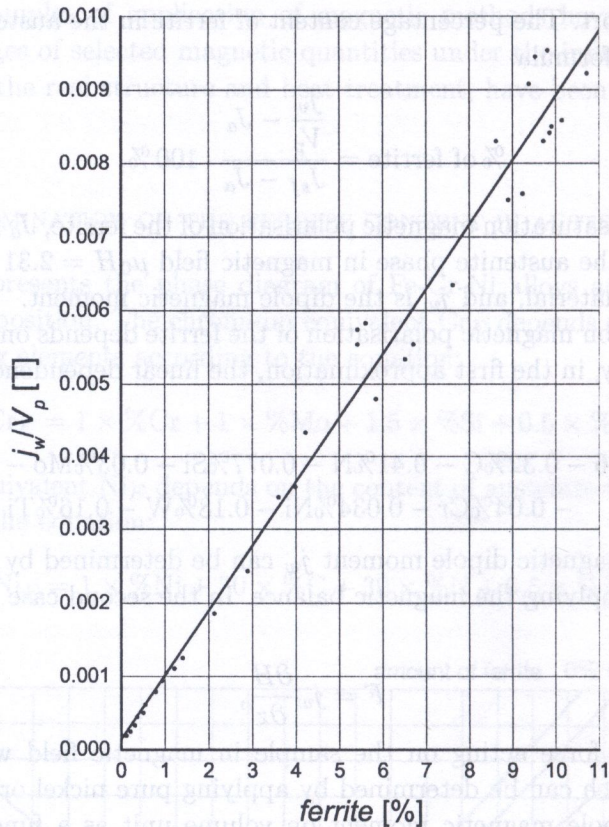


FIG. 2. Magnetic dipole moment on volume unit measured by applying magnetic balance as a function of ferrite concentration in the Fe-Cr-Ni alloys.

For higher concentration of ferrite (5%–80%), the content of this phase has been obtained by applying the X-ray diffraction method. There is a good correlation between the results achieved by magnetic and X-ray diffraction methods, whereas the magnetic method is also effectively used with large accuracy to determinate the small content of ferrite of the order of 0.1%.

### 3. MAGNETIC PHASE ANALYSIS IN LOW-CARBON AND LOW-ALLOYS STEELS

Low-carbon and low-alloys steels, used in motor transport (TRIP steels – Transformation Induced Plasticity), cooled from a suitable temperature range, can have a two-phase structure (70% of ferrite + 30% of austenite) [4–7]. Concentration of particular phases can be determined, among other structural methods, by the magnetic method. Austenite changes into martensite under the influence of plastic deformation. The magnetic method is allowed to determine the

temperatures of the beginning  $M_s$  and finish the  $M_f$  of the transformation of austenite into martensite, and the temperatures of the transformation of austenite into martensite  $M_d$  under the influence of deformation.

Figure 3 presents, for example, distribution of magnetic losses on eddy current losses  $W_w$ , hysteresis losses  $W_h$  and relaxation losses  $W_r$  for TRIP steels [4]. Similar distribution of magnetic losses can be achieved in the case of the total tangent angle of magnetic losses  $\tan \delta_{tot}$  [1, 8]

$$(3.1) \quad \tan \delta_{tot} = \tan \delta_h + \tan \delta_w + \tan \delta_r.$$

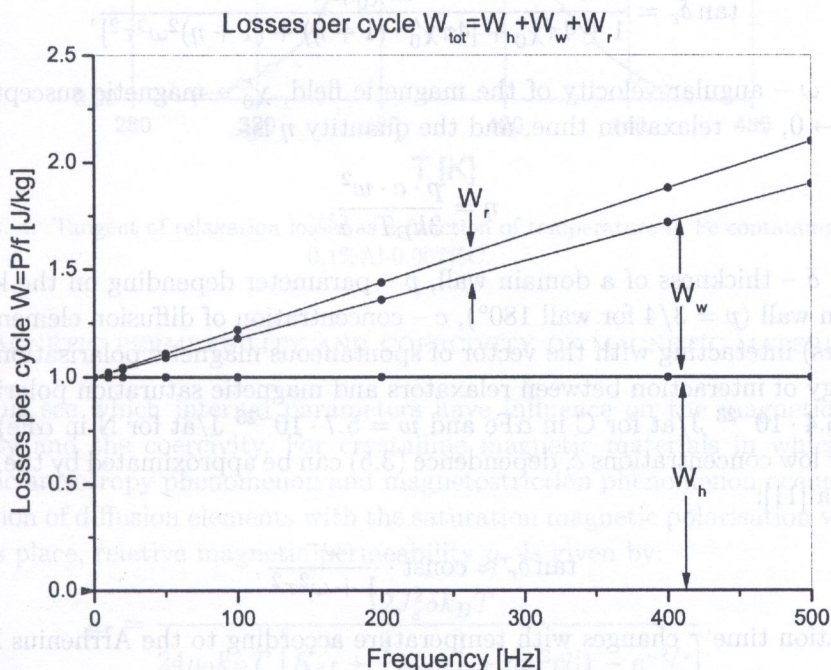


FIG. 3. Distribution of magnetic losses on eddy current losses  $W_w$ , hysteresis losses  $W_h$ , and relaxation losses  $W_r$ , for TRIP (transformation induced plasticity) steels [4].

The tangent angle of eddy current magnetic losses is given by the formula:

$$(3.2) \quad \tan \delta_w = \frac{\pi d^2 \mu_0 \mu_r f}{6\rho},$$

where  $\mu_0$  is the magnetic permeability of the vacuum,  $\mu_r$  is the relative magnetic permeability,  $f$  denotes the frequency of magnetic field,  $d$  is the thickness of the material, and  $\rho$  is the resistivity of the material.

The tangent angle of hysteresis losses in magnetic field  $H$  is given by the formula:

$$(3.3) \quad \tan \delta_h = \frac{8}{3\pi} \cdot \frac{\nu H}{\mu_p + 2\nu H},$$

where  $\nu$  is the Rayleigh constant and  $\mu_p$  is the initial relative magnetic permeability.

Additional losses (relaxation losses) resulting from interaction between diffusion elements (relaxators) and magnetic polarisation are [9, 10]:

$$(3.4) \quad \tan \delta_r = \frac{4\pi\chi'_0\eta\omega\tau}{1 + 4\pi\chi'_0 + [4\pi\chi'_0 \cdot (1 + \eta) + (1 + \eta)^2\omega^2\tau^2]},$$

where:  $\omega$  – angular velocity of the magnetic field,  $\chi'_0$  – magnetic susceptibility for  $\omega \rightarrow 0$ ,  $\tau$  – relaxation time, and the quantity  $\eta$  is:

$$(3.5) \quad \eta = \frac{p \cdot c \cdot w^2}{3k_B T \cdot \delta},$$

where:  $\delta$  – thickness of a domain wall,  $p$  – parameter depending on the kind of domain wall ( $p = 3/4$  for wall  $180^\circ$ ),  $c$  – concentration of diffusion elements (relaxators) interacting with the vector of spontaneous magnetic polarisation  $\mathbf{J}_s$ ,  $w$  – energy of interaction between relaxators and magnetic saturation polarisation ( $w = 6.4 \cdot 10^{-23}$  J/at for C in  $\alpha\text{Fe}$  and  $w = 5.7 \cdot 10^{-23}$  J/at for N in  $\alpha\text{Fe}$ ).

For low concentrations  $c$ , dependence (3.5) can be approximated by the Debye formula [11]:

$$(3.6) \quad \tan \delta_r \approx \text{const} \cdot \frac{\omega\tau}{1 + \omega^2\tau^2}.$$

Relaxation time  $\tau$  changes with temperature according to the Arrhenius law:

$$(3.7) \quad \tau = \tau_0 \exp \left[ \frac{E}{k_B T} \right],$$

where  $\tau_0$  is the preexponential factor and  $E$  is the activation energy.

For the crystalline phase, relaxation time  $\tau$  is connected with the diffusion coefficient  $D$  according to the equation:

$$(3.8) \quad D = \frac{a^2}{36\tau},$$

where  $a$  – lattice constant.

Figure 4 presents, for example, the tangent of relaxation magnetic losses angle  $\tan \delta_r$  for  $\alpha\text{Fe}-0.1\%\text{Al}-0.007\%\text{C}$ .

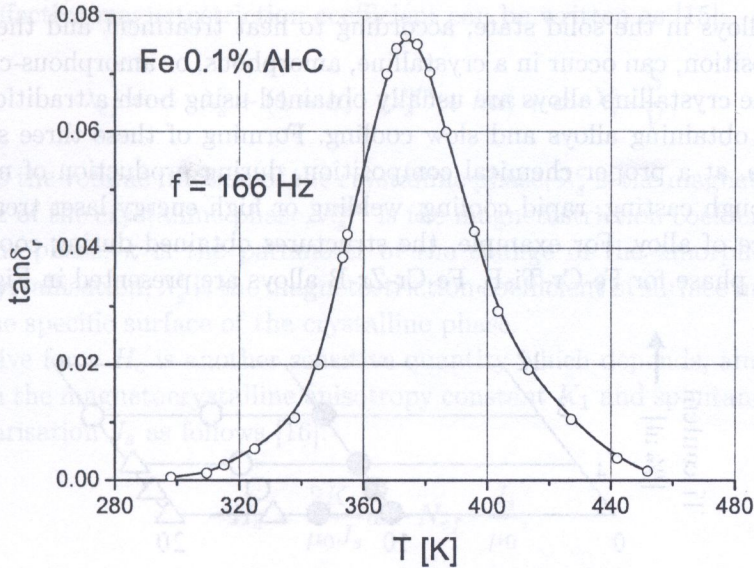


FIG. 4. Tangent of relaxation losses as a function of temperature in Fe containing 0.1%Al-0.007%C.

#### 4. MAGNETIC PERMEABILITY AND COERCIVITY OF MAGNETIC MATERIALS

Let us see which internal parameters have influence on the magnetic permeability and the coercivity. For crystalline magnetic materials in which the magnetic anisotropy phenomenon and magnetostriction phenomenon occur, and interaction of diffusion elements with the saturation magnetic polarisation vector  $J_s$  takes place, relative magnetic permeability  $\mu_r$  is given by:

$$(4.1) \quad \mu_r = \frac{12J_s^2 \delta k_B T}{24\mu_0 k_B T \left[ K_{ef} + \frac{3}{2} \lambda_{ef} \sigma \right] + pw^2 cl [1 - e^{-t/\tau}]},$$

where  $\delta$  is the thickness of the effective domain wall,  $k_B$  is the Boltzmann constant,  $T$  is temperature in the Kelvin scale,  $\mu_0$  is the magnetic permeability of vacuum,  $K_{ef}$  is the effective magnetocrystalline anisotropy constant,  $\lambda_{ef}$  is the effective magnetostriction coefficient,  $\sigma$  is stress,  $p$  is a parameter depending on the kind of domain wall,  $w$  is the interaction constant of a given diffusion element with the vector of spontaneous magnetic polarisation,  $c$  is concentration of the diffusion elements which interact with the vector of spontaneous magnetic polarisation (e.g. interstitial atoms of carbon, nitrogen, oxygen),  $l$  is the width of the effective domain,  $t$  is time counted from demagnetisation (redistribution of elements arranging themselves in one direction),  $\tau$  is the time of relaxation needed to reach the state of equilibrium of the diffusion elements (relaxators).

Iron alloys in the solid state, according to heat treatment and their chemical composition, can occur in a crystalline, amorphous, or amorphous-crystalline phase. The crystalline alloys are usually obtained using both a traditional technology of obtaining alloys and slow cooling. Forming of these three structures is possible, at a proper chemical composition, during production of machinery parts through casting, rapid cooling, welding or high energy laser treatment of the surface of alloy. For example, the structures obtained during cooling from the liquid phase for Fe-Cr-Ti-B, Fe-Cr-Zr-B alloys are presented in Fig. 5 [12].

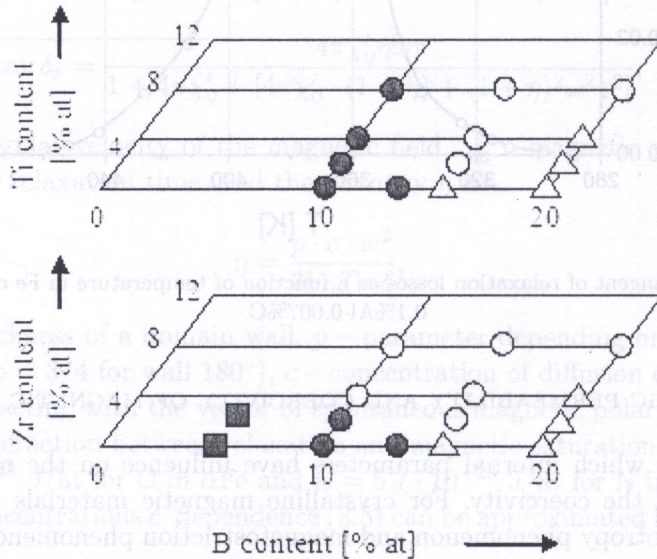


FIG. 5. Phase diagrams for Fe-Cr-(Ti/Zr)-B alloys after rapid cooling [12],  $\Delta$  - amorphous phase, one exothermal peak,  $\circ$  - amorphous phase, two exothermal peaks,  $\bullet$  - amorphous phase + crystalline phase, one exothermal peak,  $\blacksquare$  - crystalline phase.

For amorphous structure, the magnetocrystalline anisotropy constant usually is zero ( $K_{ef} = 0$ ). In the case of amorphous and crystalline phases, and when the dimensions of the crystalline phase are smaller than the magnetic exchange length, the effective magnetocrystalline constant is equal [13, 14]:

$$(4.2) \quad K_{ef} = \frac{K_1^4 d^6}{A^3},$$

where  $K_1$  is the magnetocrystalline anisotropy constant of the crystalline phase,  $d$  is the average diameter of the crystalline phase,  $A$  is the constant of exchange interaction.

For the crystalline phase:

$$(4.3) \quad K_{ef} = K_1.$$

The effective magnetostriction coefficient can be written as [15]:

$$(4.4) \quad \lambda_{ef} = \alpha \cdot \lambda_s^c + (1 - \alpha) \cdot (\lambda_s^{am} + k\alpha) + \alpha \cdot \lambda_s^s \cdot \frac{S}{V},$$

where  $\alpha$  is the volume fraction of the crystalline phase,  $\lambda_s^c$  is the magnetostriction coefficient of the crystalline phase,  $\lambda_s^{am}$  is the magnetostriction coefficient of the amorphous phase,  $k$  is the parameter of the change of the amorphous phase during crystallisation,  $\lambda_s^s$  is the magnetostriction coefficient of surface interaction,  $S/V$  is the specific surface of the crystalline phase.

Coercive force  $H_c$  is another sensitive quantity which depends, among other things, on the magnetocrystalline anisotropy constant  $K_1$  and spontaneous magnetic polarisation  $J_s$  as follows [16]:

$$(4.5) \quad H_c = \frac{2K_1}{\mu_0 J_s} a - N_{ef} \cdot \frac{J_s}{\mu_0},$$

where the parameters  $a$  and  $N_{ef}$  depend on the domain structure and microstructure of the material.

For example Fig. 6 presents the dependence of coercivity on the magnetocrystalline anisotropy constant  $K_1$  for different magnetic materials [16].

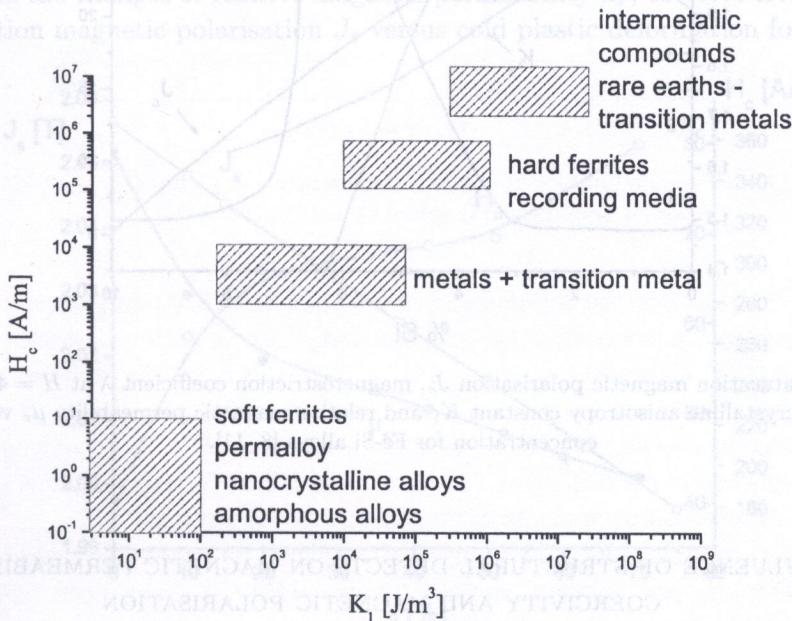


FIG. 6. Coercivity  $H_c$  of soft and hard magnetic materials as a function of the magnetocrystalline anisotropy constant  $K_1$  [16].

The changes of coercivity can also be a result of the irregularities of the surface of ferromagnetic [17]:

$$(4.6) \quad H_c^{\text{surf}} = \frac{\pi \cdot h_1 \cdot \gamma}{J_s \cdot h_0 \cdot l'}$$

where  $h_1$  is the amplitude of the change of thickness,  $\gamma$  is the energy of the domain wall of the unit of surface,  $J_s$  is the saturation magnetic polarisation,  $h_0$  is the average diameter of material,  $l'$  is the length of wave irregularity.

To illustrate the influence of the saturation magnetic polarisation  $J_s$ , the magnetostriction coefficient  $\lambda$ , and the magnetocrystalline anisotropy constant  $K_1$  on the relative magnetic permeability  $\mu_r$ , the dependence of  $\mu_r$  on the concentration of silicon in the Fe-Si alloys has been presented in Fig. 7. The experimental data in Fig. 7 confirm that  $K_1$ ,  $\lambda$  and  $\mu_r$  vary along with the Si content, and according to formula (4.1), the  $\mu_r$  has a maximum.

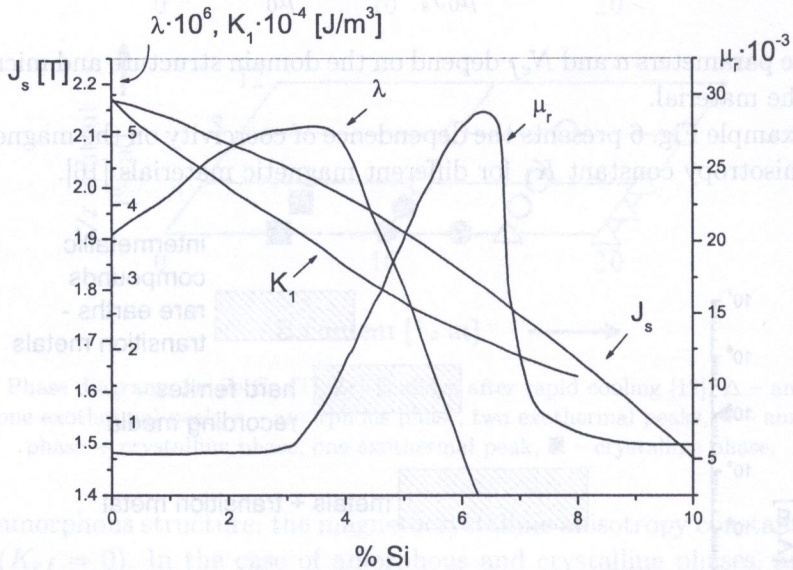


FIG. 7. Saturation magnetic polarisation  $J_s$ , magnetostriction coefficient  $\lambda$  at  $H = 40$  A/cm, magnetocrystalline anisotropy constant  $K_1$  and relative magnetic permeability  $\mu_r$  versus Si concentration for Fe-Si alloys [8, 11].

##### 5. INFLUENCE OF STRUCTURAL DEFECTS ON MAGNETIC PERMEABILITY, COERCIVITY AND MAGNETIC POLARISATION

Structural defects (vacancies and dislocations) are the preferential places of formation of micro-cracks and then of macro-cracks [18, 19]. In pure metals and

alloys, the dislocations are formed under the influence of cold plastic deformation. Figure 8 presents the dislocation structure of iron after cold plastic deformation by rolling ( $\epsilon = 5\%$  and  $\epsilon = 30\%$ ), obtained by electron microscopy.

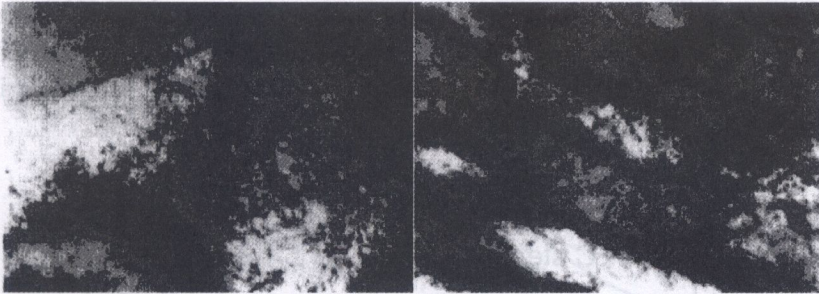


FIG. 8. Dislocation structure of iron after cold-rolling ( $\epsilon = 5\%$  and  $\epsilon = 30\%$ ) [20].

For small deformations, the dislocations have a uniform distribution, for higher deformations a non-uniform distribution of dislocations is observed. For much higher plastic deformations, a cellular structure of dislocations is formed. For higher deformations cracking take place. Changes of the dislocation structure in steels occur similarly, but for different values of deformation. Figure 9 presents the changes of relative magnetic permeability  $\mu_r$ , coercive force  $H_c$  and saturation magnetic polarisation  $J_s$  versus cold plastic deformation for iron.

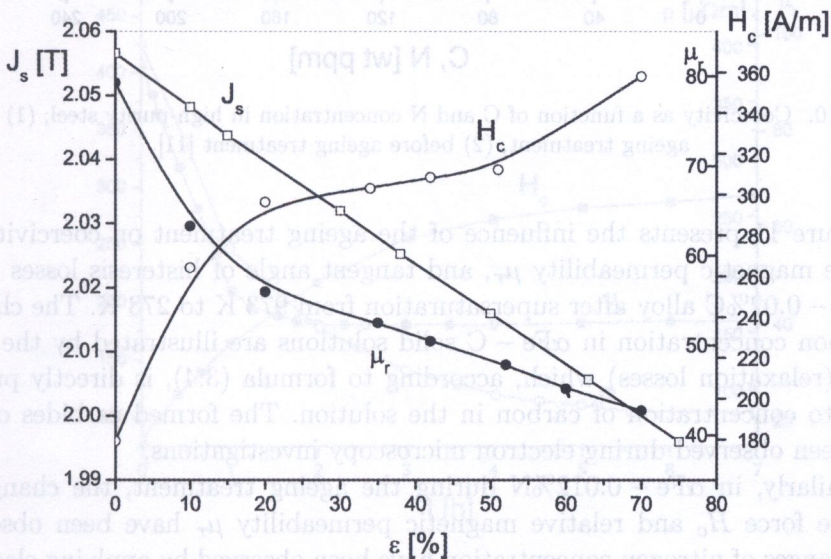


FIG. 9. Saturation magnetic polarisation  $J_s$ , relative magnetic permeability  $\mu_r$  and coercivity force  $H_c$  versus cold plastic deformation  $\epsilon$  for electrolytic iron [20].

## 6. INFLUENCE OF PRECIPITATION ON MAGNETIC PROPERTIES

The precipitations of interstitial atoms in iron alloys also leads to forming of the cracks during long-standing work under stresses [18, 19, 21]. In connection with this fact, the influence of precipitation of carbides and nitrides on the changes of magnetic parameters has been investigated. Figure 10 presents the influence of N and C contents in the solution and after ageing treatment in high purity steel [11].

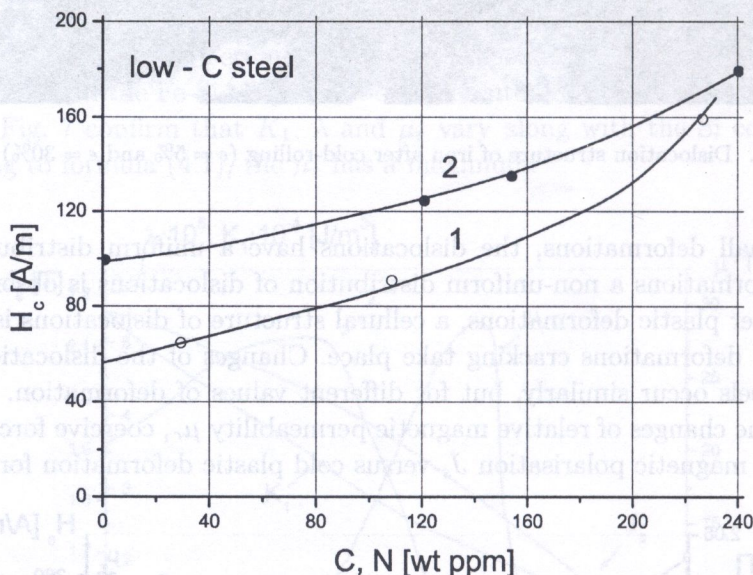


FIG. 10. Coercivity as a function of C and N concentration in high-purity steel; (1) after ageing treatment, (2) before ageing treatment [11].

Figure 11 presents the influence of the ageing treatment on coercivity  $H_c$ , relative magnetic permeability  $\mu_r$ , and tangent angle of hysteresis losses  $\tan \delta_h$  in  $\alpha\text{Fe} - 0.02\%C$  alloy after supersaturation from 973 K to 273 K. The changes of carbon concentration in  $\alpha\text{Fe} - C$  solid solutions are illustrated by the value  $\tan \delta_r$  (relaxation losses) which, according to formula (3.4), is directly proportional to concentration of carbon in the solution. The formed carbides of iron have been observed during electron microscopy investigations.

Similarly, in  $\alpha\text{Fe} - 0.012\%N$  during the ageing treatment, the changes of coercive force  $H_c$  and relative magnetic permeability  $\mu_r$  have been observed. The changes of nitrogen concentration have been observed by applying electrical resistivity  $\rho$  (Fig. 12). The formed nitrides of iron after ageing treatment have been observed by electron microscopy methods.

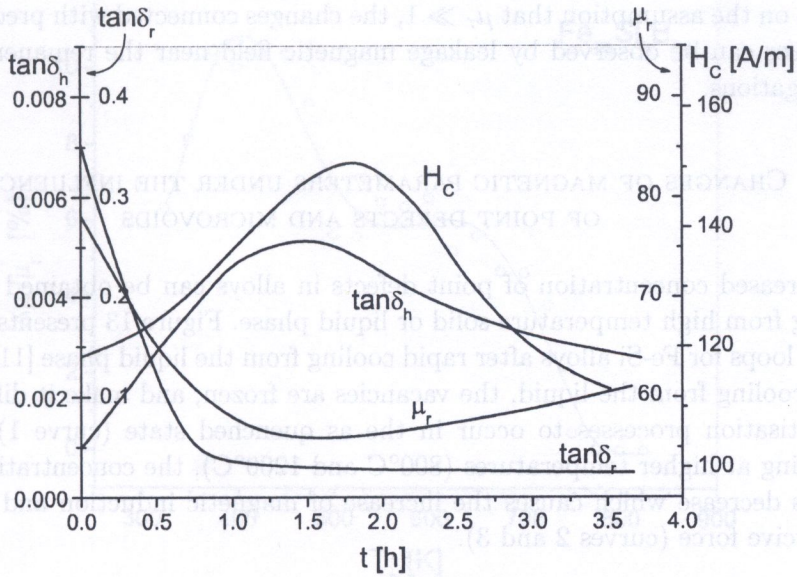


FIG. 11. Changes of coercivity  $H_c$ , relative magnetic permeability  $\mu_r$ , tangent of magnetic hysteresis losses  $\tan \delta_h$ , and relaxation magnetic losses  $\tan \delta_r$  during ageing at the temperature 523 K after supersaturation from the temperature 973 K to 273 K in  $\alpha\text{Fe} - 0.02\%C$  [20].

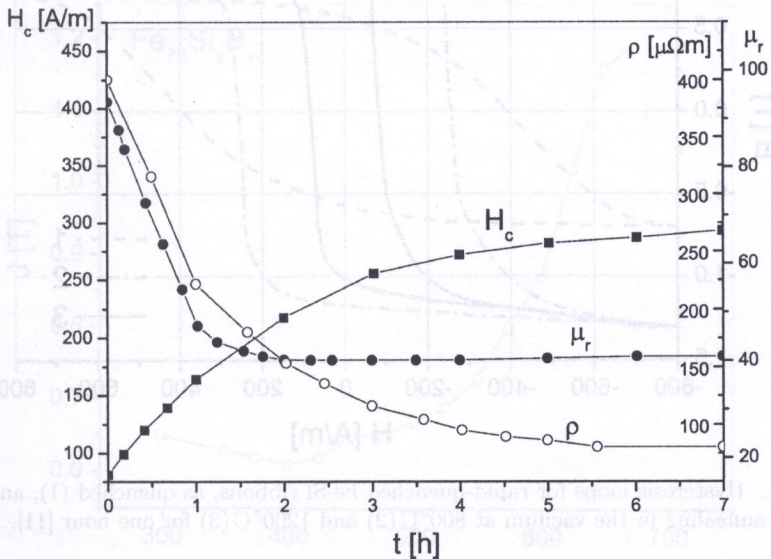


FIG. 12. Coercivity  $H_c$ , relative magnetic permeability  $\mu_r$ , and resistivity  $\rho$  measured at room temperature versus aging time  $t$  at the temperature 423 K after supersaturation from 863 K to 273 K in  $\alpha\text{Fe} - 0.012\%N$  [20].

Because magnetisation is proportional to magnetic susceptibility  $\chi$  ( $\chi = \mu_r - 1$ ) on the assumption that  $\mu_r \gg 1$ , the changes connected with precipitation processes can be observed by leakage magnetic field near the remanence point investigations.

#### 7. CHANGES OF MAGNETIC PARAMETERS UNDER THE INFLUENCE OF POINT DEFECTS AND MICROVOIDS

Increased concentration of point defects in alloys can be obtained by rapid cooling from high temperature solid or liquid phase. Figure 13 presents the hysteresis loops for Fe-Si alloys after rapid cooling from the liquid phase [11]. During rapid cooling from the liquid, the vacancies are frozen, and make it difficult for magnetisation processes to occur in the as quenched state (curve 1). During annealing at higher temperatures (800°C and 1200°C), the concentration of vacancies decrease which causes the increase of magnetic induction and decrease of coercive force (curves 2 and 3).

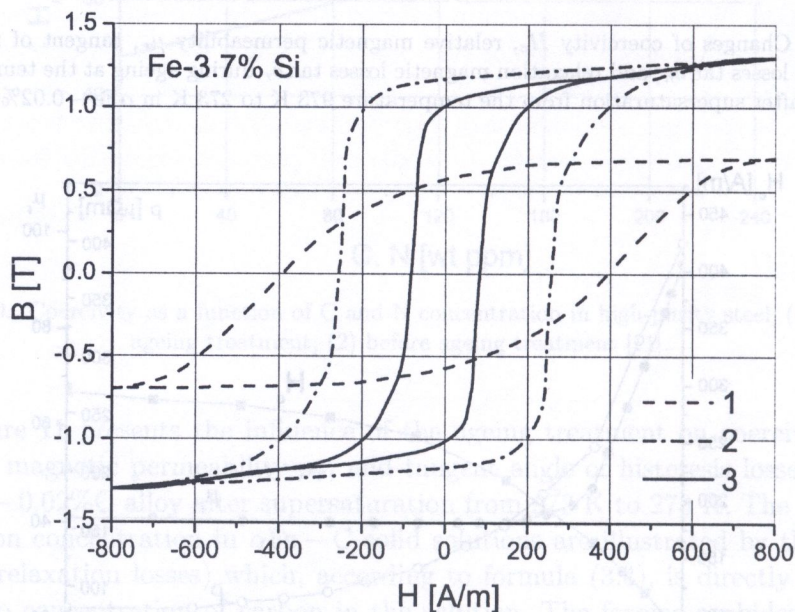


FIG. 11. Hysteresis loops for rapid-quenched Fe-Si ribbons, as quenched (1), and after annealing in the vacuum at 800°C (2) and 1200°C (3) for one hour [11].

Similarly, in amorphous alloys obtained by melt spinning method, microvoids are frozen (Fig. 14). During annealing of the material for one hour at elevated temperatures  $T_a$ , the decrease of microvoid concentration takes place. The con-

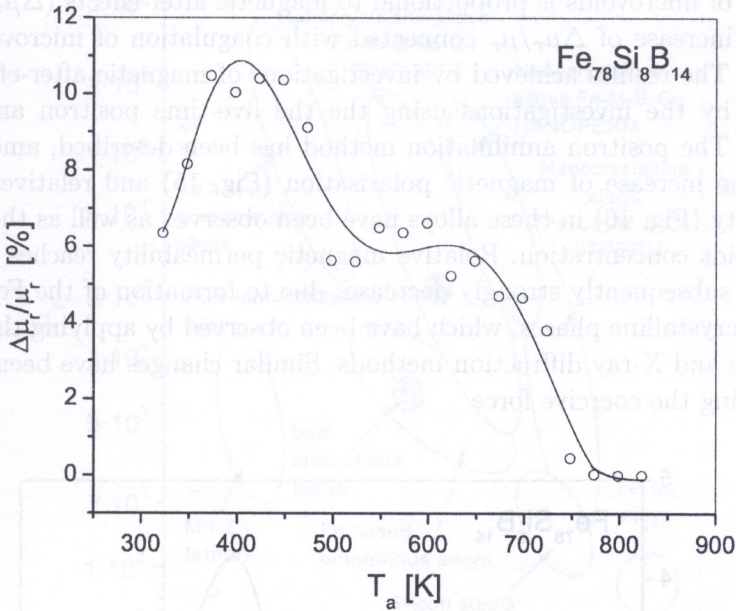


FIG. 12. Changes of magnetic after-effects  $\Delta\mu_r/\mu_r$  versus one-hour annealing temperature  $T_a$  for Fe<sub>78</sub>Si<sub>8</sub>B<sub>14</sub> alloy.

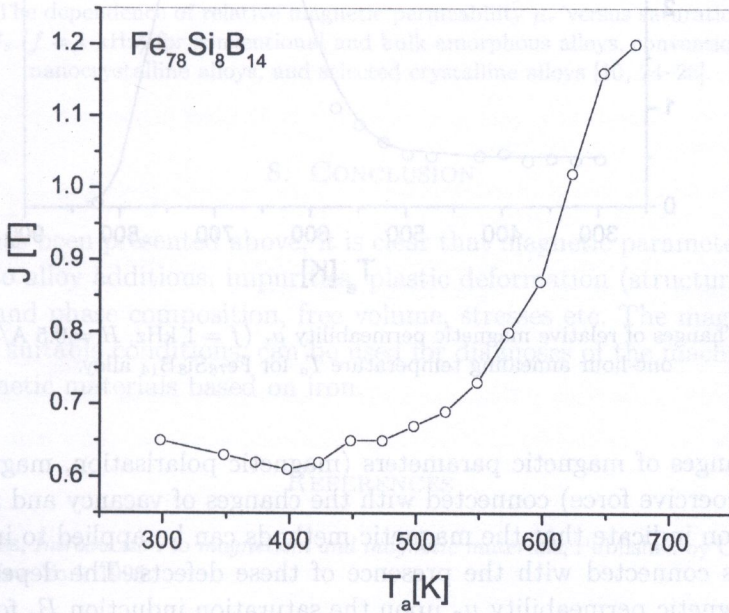


FIG. 13. Changes of magnetic polarisation versus one-hour annealing temperature  $T_a$  for Fe<sub>78</sub>Si<sub>8</sub>B<sub>14</sub> alloy.

centration of microvoids is proportional to magnetic after-effects ( $\Delta\mu_r/\mu_r$ ). Initially, the increase of  $\Delta\mu_r/\mu_r$  connected with coagulation of microvoids takes place [22]. The results achieved by investigations of magnetic after-effects were confirmed by the investigations using the the live-time positron annihilation technique. The positron annihilation method has been described, among them, in [23]. The increase of magnetic polarisation (Fig. 15) and relative magnetic permeability (Fig. 16) in these alloys have been observed as well as the decrease of microvoids concentration. Relative magnetic permeability reaches the maximum, and subsequently strongly decreases due to formation of the  $\text{Fe}_2\text{B}$ ,  $\text{Fe}_3\text{B}$ , and  $\text{Fe}_3\text{Si}$  crystalline phases, which have been observed by applying the electron microscope and X-ray diffraction methods. Similar changes have been observed by measuring the coercive force.

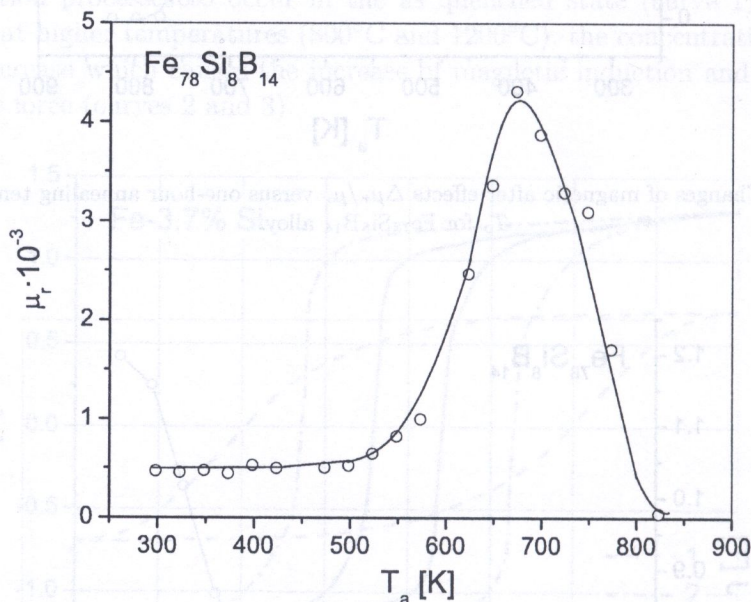


FIG. 14. Changes of relative magnetic permeability  $\mu_r$  ( $f = 1$  kHz,  $H = 0.5$  A/m versus one-hour annealing temperature  $T_a$  for  $\text{Fe}_{78}\text{Si}_8\text{B}_{14}$  alloy.

The changes of magnetic parameters (magnetic polarisation, magnetic permeability, coercive force) connected with the changes of vacancy and microvoid concentration indicate that the magnetic methods can be applied to investigate the changes connected with the presence of these defects. The dependence of relative magnetic permeability  $\mu_r$  upon the saturation induction  $B_s$  for conventional and bulk amorphous alloys, conventional and bulk nanocrystalline alloys and crystalline materials, has been presented in Fig. 17 [10, 24–26].

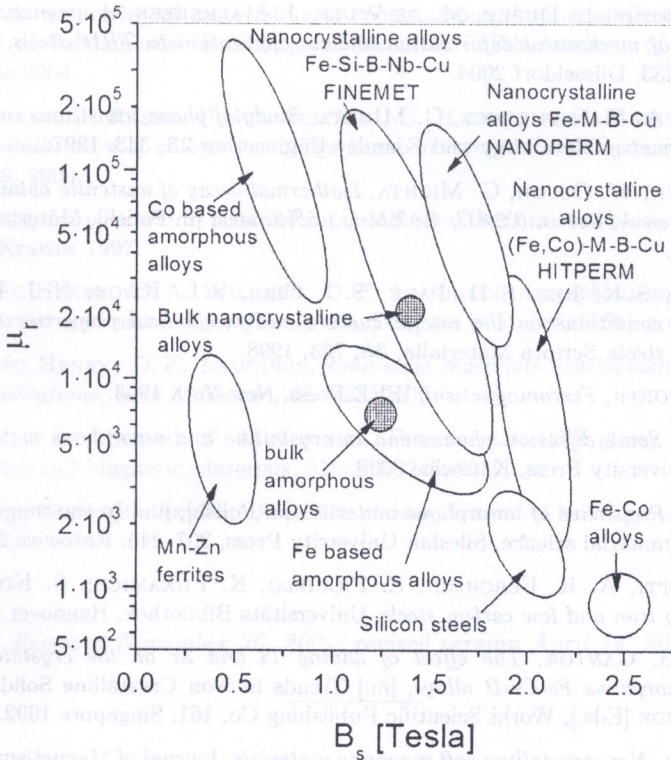


FIG. 15. The dependence of relative magnetic permeability  $\mu_r$  versus saturation magnetic induction  $B_s$  ( $f = 1$  kHz) for conventional and bulk amorphous alloys, conventional and bulk nanocrystalline alloys, and selected crystalline alloys [10, 24–26].

### 8. CONCLUSION

As it has been presented above, it is clear that magnetic parameters are very sensitive to alloy additions, impurities, plastic deformation (structural defects), chemical and phase composition, free volume, stresses etc. The magnetic parameters, in suitable conditions, can be used for diagnoses of the machinery made from magnetic materials based on iron.

### REFERENCES

1. D. JILES, *Introduction to magnetism and magnetic materials*, Published by Chapman and Hall, New York 1996.
2. H. RAWA, *Electricity and magnetism in technique* [in Polish], PWN, Warszawa 2001.
3. L. A. DOBRZAŃSKI, *Metallic engineering materials* [in Polish], WNT, Warszawa 2002.

4. L. VANDEBOSHE, L. DUPRE, M. DE WULF, J. MALKEBEEK, *A magnetic technique for evaluation of mechanical deformation and its application to TRIP-steels*, Soft magnetic materials, 233, Düsseldorf 2004.
5. PIETRZYK, A. MAKSYMOWICZ, G. MICHTA, *Study of phase transitions in steel by means of magnetometry*, Metallurgy and Foundry Engineering **23**, 343, 1997.
6. J. PIETRZYK, W. OSUCH, G. MICHTA, *Isothermal decay of austenite obtained in temperature between A3-A1 in 0.2%C, 1.5%Mn, 1.5%Si steel* [in Polish], Materials Engineering **1**, 18, 1998.
7. H. J. KOH, S. K. LEE, S. H. PARK, S. J. CHOI, S. L. KWON, N. J. KIM, *Effect of hot rolling conditions on the microstructure and mechanical properties of Fe-C-Mn-Si multiphase steels*, Scripta Materialia, **38**, 763, 1998.
8. R. M. BOZORTH, *Ferromagnetism*, IEEE Press, New York 1993.
9. J. RASEK, *Some diffusion phenomena in crystalline and amorphous metals* [in Polish], Silesian University Press, Katowice 2000.
10. J. RASEK, *Properties of amorphous materials* [in Polish], [in:] In the range of crystallography and material science, Silesian University Press, 207–245, Katowice 2002.
11. G. BERTOTTI, A. R. FERCHMIN, E. FIORILLO, K. FUKAMICHI, S. KOBE, S. ROTH, *High purity iron and low carbon steels*, Universitäts Bibliothek, Hannover 1994.
12. K. ISHI, B. CANTOR, *The effect of adding Ti and Zr on the crystallization behaviour of amorphous Fe-Cr-B alloys*, [in:] Trends in Non Crystalline Solids, A. CONDE, C. F. CONDE [Eds.], World Scientific Publishing Co, 161, Singapore 1992.
13. G. HERZER, *Nanocrystalline soft magnetic materials*, Journal of Magnetism and Magnetic Materials, 157/158, 133, 1996.
14. G. HERZER, L. L. VARGA, *Exchange softening in nanocrystalline alloys*, Journal of Magnetism and Magnetic Materials, 215/215 506, 2000.
15. A. ŚLAWSKA-WANIEWSKA, *Interface magnetism in Fe-based nanocrystalline alloys*, Journal de Physique IV, **8**, 11, 1998.
16. H. KRONMÜLLER, *Recent developments in high-tech magnetic materials*, Journal of Magnetism and Magnetic Materials, **25**, 140–144, 1995.
17. H. KRONMÜLLER, *Theory of the coercive field in amorphous ferromagnetic alloys*, Journal of Magnetism and Magnetic Materials, **24**, 159, 1981.
18. G. SOCHA, *New method of detection and monitoring of initial stages of the fatigue accumulation in constructional steels* [in Polish], Lapromat-Centre of Excellence, Institute of Fundamental Technological Research, Polish Academy of Sciences, Warszawa 2004.
19. L. DIETRICH, *Development of structural damage and assessment of a state of material degradation* [in Polish], [in:] Proceedings of Conference Testing of mechanical properties of materials and constructions, Lapromat-Centre of Excellence, Institute of Fundamental Technological Research, Polish Academy of Sciences, p. 9, Zakopane 2004.
20. J. RASEK, *The kinetics of precipitation and resolution phenomena in Fe-N(C) solid solutions* [in Polish], Silesian University, Katowice 1983.
21. B. AUGUSTYNIAK, *Magnetic methods of nondestructive assessment of microstructure of steels exploited at power plants* [in Polish], [in:] Proceedings of Conference Testing of

- mechanical properties of materials and constructions, Lapromat-Centre of Excellence, Institute of Fundamental Technological Research, Polish Academy of Sciences, p. 209, Zakopane 2004.
22. Z. STOKŁOSA, J. RASEK, P. KWAPULIŃSKI, G. HANECZOK, G. BADURA, J. LELATKO, *Nanocrystallisation of amorphous alloys based on iron*, Material Science and Engineering C, **23**, 49, 2003.
  23. J. DRYZEK, *Introduction to positron annihilation methods in solid state*, Jagiellonian University, Kraków 1997.
  24. M. E. MC HENRY, M. A. WILLARD, D. E. LAUGHLIN, *Amorphous and nanocrystalline materials for applications as soft magnets*, Progress in Materials Science, **44**, 291, 1999.
  25. M. E. MC HENRY, D. E. LAUGHLIN, *Nano-scale materials development for future magnetic applications*, Acta Materiala, **48**, 223, 2000.
  26. A. INNOUE, A. MAKINO, T. MUZUSHIMA, *Ferromagnetic bulk glassy alloys*, Journal of Magnetism and Magnetic Materials, 215/216, 246, 2000.
  27. T. KULIK, *Nanocrystallization of metallic glasses*, Journal of Non-Crystalline Solids, **287**, 145, 2001.

Received November 30, 2004; revised version April 12, 2005.

## 1. INTRODUCTION

The use of fibre reinforced composite materials in modern engineering structural design has become a common practice. However, since more design variables typically exist when composite materials are employed and the manufacturing processes for producing composites are more complex, more variability can exist in a design produced with composites compared to conventional materials. Thus, the variability of properties that occur in composite structures leads directly to a random field of variables describing constructions. A scatter of properties has a different origin, but, in general, it may be divided and classified in the following manner: (1) geometric properties (imperfections), (2) physical and mechanical properties, (3) environmental effects (exploitation), (4) technology (understood in the range of geometrical dimensions but as an origin of local defects - a scatter of fibre directions etc.). Therefore, there is a fundamental question: how many and which of the above factors can (or should) be incorporated in the design process and how can we manage to take into account the existing variability of parameters.

Although the majority of available references in literature discussing the design problems of composite structures is devoted to the analysis conducted in a pure deterministic way, the variety of methods exists that have been adopted in